

Tunable Quantum Anomalous Hall Effects in Ferromagnetic van der Waals Heterostructures

Feng Xue^{1,2}, Yusheng Hou³, Zhe Wang⁴, Zhiming Xu², Ke He^{1,2,5}, Ruqian Wu⁶, Yong Xu^{2,5,7,8,*}, Wenhui Duan^{1,2,5,9,*}

¹ Beijing Institute of Quantum Information Science, Beijing 100193, China

² State Key Laboratory of Low-Dimensional Quantum Physics, Department of Physics, Tsinghua University, Beijing 100084, China

³ Guangdong Provincial Key Laboratory of Magnetoelectric Physics and Devices, Center for Neutron Science and Technology, School of Physics, Sun Yat-Sen University, Guangzhou, 510275, China

⁴ State Key Laboratory of Surface Physics and Key Laboratory for Computational Physical Sciences (MOE) and Department of Physics, Fudan University, Shanghai 200433, China

⁵ Frontier Science Center for Quantum Information, Beijing 100084, China

⁶ Department of Physics and Astronomy, University of California, Irvine, CA 92697-4575, USA

⁷ Tencent Quantum Laboratory, Tencent, Shenzhen, Guangdong 518057, China

⁸ RIKEN Center for Emergent Matter Science (CEMS), Wako, Saitama 351-0198, Japan

⁹ Institute for Advanced Study, Tsinghua University, Beijing 100084, China

ABSTRACT

The quantum anomalous Hall effect (QAHE) has unique advantages in topotronic applications, but it is still challenging to realize the QAHE with tunable magnetic and topological properties for building functional devices. Through systematic first-principles calculations, we predict that the in-plane magnetization induced QAHE with Chern numbers $C = \pm 1$ and the out-of-plane magnetization induced QAHE with high Chern numbers $C = \pm 3$ can be realized in a single material candidate, which is composed of van der Waals (vdW) coupled Bi and MnBi_2Te_4 monolayers. The switching between different phases of QAHE can be controllable by multiple ways, such as applying strain or (weak) magnetic field or twisting the vdW materials. The prediction of an experimentally available material system hosting robust, highly tunable

QAHE will stimulate great research interest in the field. Our work opens a new avenue for the realization of tunable QAHE and provides a practical material platform for the development of topological electronics.

* Corresponding authors: duanw@tsinghua.edu.cn; yongxu@mail.tsinghua.edu.cn;

INTRODUCTION

The quantum anomalous Hall effect (QAHE), featured by a quantized Hall conductance at zero magnetic field and the topologically protected chiral edge states, has been widely studied in recent years [1-3]. Typically, an out-of-plane magnetization is needed to break the time reversal symmetry and all in-plane mirror symmetries. To this end, most prior theoretical and experimental work have been pursuing QAHE in materials with an out-of-plane magnetization (OPM-QAHE) [4-12]. Nevertheless, QAHE can also be induced by an in-plane magnetization, i.e., IPM-QAHE, as revealed by Liu *et al.* in 2013 based on two-dimensional (2D) point group symmetry analysis [13]. It is known that most magnetic films prefer in-plane magnetic anisotropy as the thickness is reduced to a few monolayers [14-17], so it is more appealing to establish QAHE in geometries with in-plane magnetization for their integration in nanodevices. The main hurdle for the realization of IPM-QAHE is that the in-plane magnetization does not necessarily break all symmetries that can forbid the anomalous Hall conductance in most materials and this research area hence has not been much explored [13,18-22]. Furthermore, the search for topological materials with high and tunable Chern numbers is another attractive interdisciplinary fundamental topic as the multiple dissipationless edge conduction channels may significantly improve the performance of devices [23]. It is believed that materials with high-Chern-numbers lead to new topological phases with exotic elementary excitations [24]. Therefore, finding innovative material platforms for experimental realization of IPM-QAHE, preferably also with multiple quantum edge states, is crucial for the advance of topotronic physics and applications.

Given that research of van der Waals (vdW) magnets are rapidly advancing [25-29] and their magnetization can be conveniently controlled by bias or strain [30], it is intriguing to explore QAHE in ferromagnetic (FM) vdW heterostructures. Unlike many magnetic insulators with unwanted hybridization and charge transfer at their interfaces with topological insulators (TIs), 2D vdW magnets safeguard the topological surface

states (TSSs) and it appears to be an excellent strategy to delve into heterostructures with different FM vdW films and TIs for the realization of QAHE at a reasonably high temperature. What's more, it is also intriguing and meaningful to explore if IPM-QAHE and OPM-QAHE may coexist and switchable in these heterostructures. This is expected to greatly enrich the pool of topological quantum materials and provide new ideas for the design of multifunctional topological devices.

In this work, we theoretically explore the electronic, magnetic and topological properties of the vdW heterostructure of ferromagnetic MnBi_2Te_4 septuple layer (SL) and nonmagnetic Bi bilayer (BL), as depicted in Fig. 1(a). Through first-principles calculations, we demonstrate that IPM-QAHE with Chern numbers $C = \pm 1$ as well as OPM-QAHE with Chern numbers $C = \pm 3$ can be realized in the Bi/ MnBi_2Te_4 heterostructure. As a strain of 2-3% can flip the magnetization from in-plane to out-plane, topological phase transition between the two QAHE states is easily accessible. Moreover, the system may switch between $C = +3$ and $C = -3$ phases by simply twisting the FM layers in the heterostructure by 60° without need of an external magnetic field to reverse the spin direction. The controllable magnetism and topological phase transition in this ferromagnetic vdW heterostructure are illustrated in Fig. 1(b). This work provides a unique material platform for the realization and manipulation of multiple QAHE phases as required in tunable nanodevices.

RESULTS

Structural and magnetic properties

The bulk Bi and MnBi_2Te_4 crystallize in the same rhombohedral layered structure with the space group $R\bar{3}m$, and the layers stack along the perpendicular direction with an ABC sequence. The MnBi_2Te_4 monolayer consists of a Te-Bi-Te-Mn-Te-Bi-Te SL, wherein Mn atoms are arranged in a triangular lattice with spins parallel to each other. The single layer of Bi in a honeycomb lattice has a buckled structure, with the nearest atoms displacing in the perpendicular direction, and thus it is usually called BL in the literature. Bi BL is a topological insulator with the band gap of 0.47 eV by either GGA+U or HSE06 calculations [Fig. S1a (S1c)]. The MnBi_2Te_4 SL is a FM semiconductor with a band gap of 0.19 eV (0.56 eV) by GGA+U (HSE06) calculations [Fig. S1b (S1d)]. The optimized lattice constants of the MnBi_2Te_4 SL and Bi BL with

the inclusion of the spin-orbit coupling (SOC) effect are 4.37 and 4.38 Å, respectively, consistent with previous theoretical results [31, 32]. Such a good lattice match is advantageous for experimental synthesis of Bi/MnBi₂Te₄ heterostructure.

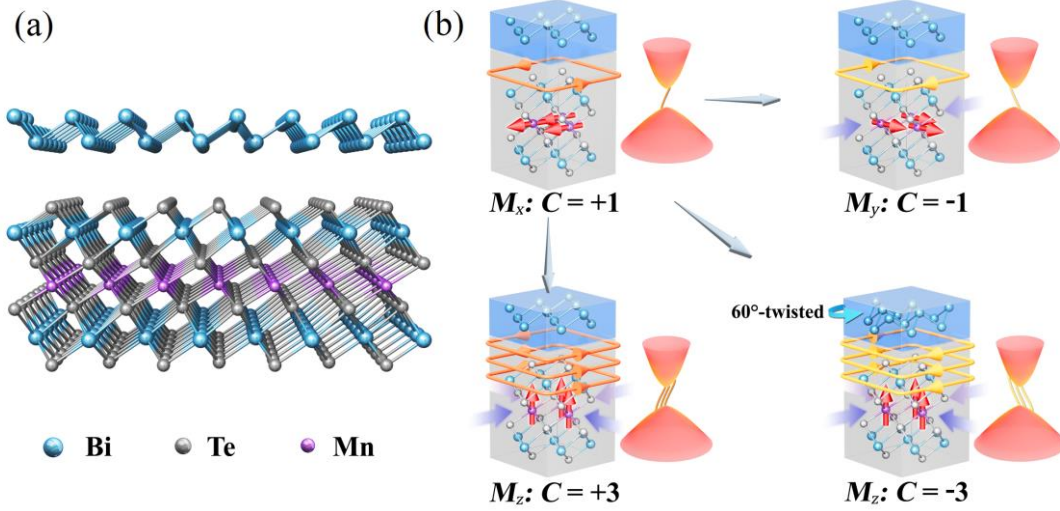


FIG 1. (a) Crystal structure of Bi/MnBi₂Te₄ vdW heterostructure. (b) Schematic diagram showing controllable magnetism and topological phase transition in the material. The magnetization orientation (M_i ; $i = x, y, z$; red arrows) is tunable by applying strain (denoted by purple arrows) or magnetic field. QAH states with controllable Chern numbers are realized by changing the magnetization orientation or twisting the vdW heterostructure.

There are six possible high-symmetry alignments between MnBi₂Te₄ SL and Bi BL in the Bi/MnBi₂Te₄ heterostructure. As shown in Fig. S2, three of them have the inner Bi atoms of Bi BL sitting above the hollow, Te and Bi sites of MnBi₂Te₄ (denoted as P1, P2 and P3, respectively). The other three alignments are obtained by twisting the Bi BL by 60° (denoted as P1', P2' and P3'). According to their binding energies in Table S2, the most stable configuration is the P1 structure depicted in Figs. 1(a) and S2(a). The optimized interlayer distance between MnBi₂Te₄ SL and Bi BL is 2.84 Å, a value which is comparable to that (2.73 Å) between adjacent SLs in bulk MnBi₂Te₄ [33], indicating that the interaction between MnBi₂Te₄ SL and Bi BL is also of the vdW type. Indeed, the calculated binding energy (E_b) is only -0.402 eV/unit cell for the most preferred P1 structure. Here, the binding energy is define as $E_b = E_{Bi/MnBi_2Te_4} - E_{Bi} - E_{MBT}$, with E_{Bi} , $E_{MnBi_2Te_4}$ and $E_{Bi/MnBi_2Te_4}$ representing the energies of

isolated Bi BL, MnBi₂Te₄ SL and Bi/MnBi₂Te₄ heterostructure, respectively. Similar to the free-standing MnBi₂Te₄ SL, the exchange interaction between the nearest neighbor Mn²⁺ ions in Bi/MnBi₂Te₄ is FM and its value is 1.08 meV (Table S1). This indicates that MnBi₂Te₄ retains its FM ground state in Bi/MnBi₂Te₄. Noticeably, the magnetic easy axis of Bi/MnBi₂Te₄ is changed to in-plane, with a tiny magnetic anisotropy energy (MAE) of $E_x - E_z = -0.15$ meV/Mn (Fig. S3). This is different from the out-of-plane magnetic easy axis of the free-standing MnBi₂Te₄ SL. Further calculations show that the energy barrier of spin rotation within the x - y plane is negligibly small (Fig. S3), indicating that the Bi/MnBi₂Te₄ is a typical 2D XY magnets. In such easy-plane 2D systems, the magnetic order can be stabilized by the finite size effect as has been demonstrated recently in 1T-VSe₂ and CrCl₃ monolayers [17,34].

In-plane magnetization induced QAHE

The in-plane magnetic Bi/MnBi₂Te₄ heterostructure provides an interesting platform for exploring the IPM-QAHE. As known, all in-plane mirror symmetries must be broken for the realization of QAHE since they forbid the anomalous Hall conductance. While this symmetry breaking can be naturally achieved in geometries with an out-of-plane magnetization, the circumstance needs to be carefully checked for IPM-QAHE geometries. In principle, an in-plane magnetization \mathbf{m} cannot break the mirror plane M_m perpendicular to \mathbf{m} . The present Bi/MnBi₂Te₄ system has three mirror planes M_y , M_1 and M_2 , which are related to each other via the C_{3z} rotations as displayed in Fig. 2(e). Hence, the QAHE is allowed only when the in-plane magnetization is not perpendicular to any of them.

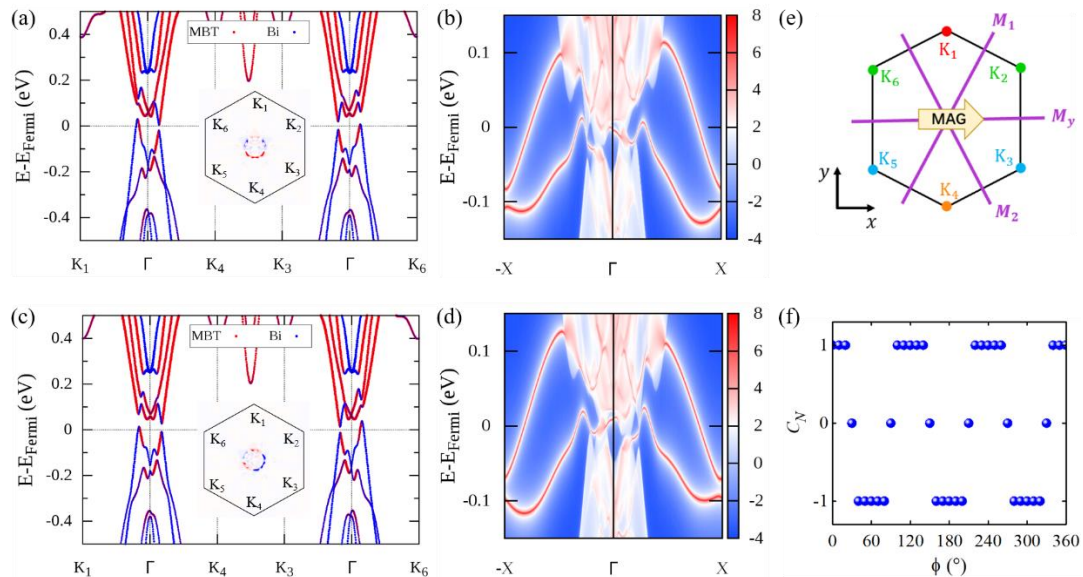


FIG 2. (a) and (c) DFT calculated band structures along the path of $K_1 \rightarrow \Gamma \rightarrow K_4 \rightarrow K_3 \rightarrow \Gamma \rightarrow K_6$ for in-plane magnetization along $\phi = 0^\circ$ and $\phi = 60^\circ$, respectively. The red and blue lines represent the components of MnBi_2Te_4 and Bi, respectively. Inset shows the distribution of Berry curvature in the first BZ. (b) and (d) The edge states corresponding to (a) and (c), respectively. (e) The first BZ of Bi/ MnBi_2Te_4 . The three violet lines denote the three mirror planes M_y , M_1 and M_2 . The magnetization is aligned to the x direction. The six K points are marked by dots. Same colors indicate that they are related by the $M_y \otimes \mathcal{T}$ symmetry operation. (f) The Chern number as a function of the in-plane magnetization direction, where ϕ is the angle between the magnetization and x direction.

To fulfil this requirement, we align the magnetization of Bi/ MnBi_2Te_4 heterostructure along the x direction (parallel to the M_y plane) and calculate its band structure and topological properties. As shown in Fig. 2(e), when the magnetization is along the x direction ($\phi = 0^\circ$), there are four nonequivalent K points in the first Brillouin zone (BZ), denoted as K_1 , K_4 , K_3 and K_6 . Owing to the preserved $M_y \otimes \mathcal{T}$ operation, K_2 and K_5 are equivalent to K_6 and K_3 , respectively. Figure 2(a) shows the component-resolved band structure along the path of $K_1 \rightarrow \Gamma \rightarrow K_4 \rightarrow K_3 \rightarrow \Gamma \rightarrow K_6$. One may see that the bands near the gap have strong intermixing between MnBi_2Te_4 and Bi. Although there is no global band gap, the electron and hole pockets are very tiny, which is also supported by calculations with the HSE06 functional (Fig. S4). The distribution of Berry curvature in the first BZ is shown in the inset of Fig. 2(a), which yields a Chern number of $C = +1$. Clearly, this means that Bi/ MnBi_2Te_4 can offer an opportunity of realizing the IPM-QAHE. This is further confirmed by the existence of one chiral edge state that connects the conduction and valence bands of a Bi/ MnBi_2Te_4 ribbon [Fig. 2(b)]. By rotating the magnetization orientation to $\phi = 60^\circ$, the band structure, shown in Fig. 2(c), looks the same as that of $\phi = 0^\circ$, except that the paths are reversed. Consequently, the sign of Berry curvature around Γ point in the first BZ changes from positive (Inset of Fig. 2a) to negative (Inset of Fig. 2c), giving a negative Chern number of $C = -1$ and one chiral edge state propagating in the opposite direction (Fig. 2d). As the magnetic energy in the x - y plane is nearly isotropic (Fig. S3), the magnetization can be rotated in the base plane

by applying a tiny magnetic field or uniaxial strain.

In addition, we calculate the Chern number of Bi/MnBi₂Te₄ as a function of the in-plane magnetization direction, and show the results in Fig. 2(f) and Fig. S5. As expected, when the in-plane magnetization is perpendicular to one of the three mirror planes (i.e., $\phi = 30^\circ + n \times 60^\circ$, with $n = 0, 1, 2, 3, 4, 5$), the Chern number drops to zero due to the preservation of mirror symmetries (Figs. S5b and S5f). Furthermore, the Chern number exhibits a periodic jumping between $C = +1$ and $C = -1$ with an interval of 60° when we rotate the magnetization in the lateral plane (Fig. S5), which is a common feature of the in-plane magnetization-induced QAHE [13,19,20,22]. The opposite Chern numbers with an interval of 60° can be explained by imposing a time reversal operation \mathcal{T} and then a 120° clockwise rotation on ϕ .

Out-of-plane magnetization induced QAHE

For device applications, it is more interesting to see if the IPM-QAHE of the Bi/MnBi₂Te₄ heterostructure can be further tuned by simple approaches, such as external magnetic fields, strain and interlayer twisting. In section A we have shown that the Bi/MnBi₂Te₄ has a tiny MAE of -0.15 meV/Mn, indicating its magnetization can be easily switched between in-plane and out-of-plane states by applying a perpendicular magnetic field. In addition, as the interaction between the MnBi₂Te₄ and Bi layers is of weak vdW type, one may twist them to a desired angle. We explore the effect of these two factors separately below.

When the spin is aligned to the z direction by applying an out-of-plane magnetic field, there are only two nonequivalent K points in the first BZ, namely K_1 and K_4 . For the most stable P1 configuration of Bi/MnBi₂Te₄ with an out-of-plane magnetization, the band structure along the path of $K_1 \rightarrow \Gamma \rightarrow K_4 \rightarrow M \rightarrow \Gamma$ is plotted in Fig. 3(a). Compared with bands of in-plane magnetization in Fig. 2(a), a noticeable change is the appearance of a global direct band gap. We then examine the topological properties by calculating the distribution of Berry curvature in the first BZ and the anomalous Hall conductivity (AHC) $\sigma_{xy} = C \frac{e^2}{h}$ (h is the Planck constant and e is the elementary charge). As illustrated in Fig. 3(b), the out-of-plane magnetization leads to a high Chern number of $C = +3$ in the band gap, with large Berry curvature values around the Γ point. In Fig.

3(c), three chiral edge states can be clearly observed for one-dimensional Bi/MnBi₂Te₄ nanoribbon, further demonstrating it is tuned to the OPM-QAHE phase with a high Chern number $C = +3$.

We next turn to the effect of twisting angles. By twisting the P1 configuration of Bi/MnBi₂Te₄ by 60°, we arrive at the P1' configuration as shown in Fig. S2(d). The main difference between these two structures is the position of the outmost atoms of Bi BL. For the P1 configuration, the outmost Bi atoms sit above the interfacial Bi atoms. While for the P1' configuration, they move to the top of interfacial Te atoms. Such a structural change leads to a significant modification of the band structure around the Fermi level [Figs. 3(a) and 3(d)], resulting in a sign change of the Berry curvature around the Γ point [Insets of Figs. 3(b) and 3(e)]. The integration of Berry curvature over the whole BZ gives a Chern number of $C = -3$, which again is confirmed by the result of quantized AHC σ_{xy} with $C = -3$ [Fig. 3(e)] in the band gap, as well as the presence of three chiral gapless edge modes from the calculation for a ribbon [Fig. 3(f)]. Herein, a 3% (-3%) strain is applied to P1 (P1') configuration to clearly show the plateau of anomalous Hall conductivity (AHC), which does not change their intrinsic topological properties.

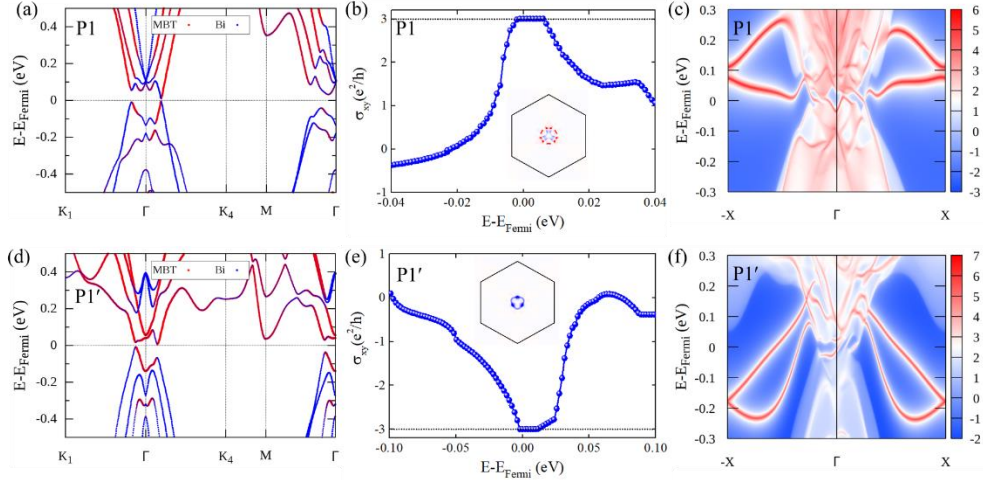


FIG 3. Topological properties of P1 (P1') configuration of Bi/MnBi₂Te₄ with an out-of-plane magnetization under a 3% (-3%) strain. (a) DFT calculated DFT band structure for P1 configuration. (b) AHC as a function of the Fermi energy for P1 configuration, where the distribution of Berry Curvature in the first BZ is shown in the inset. (c) The

chiral edge states of one-dimensional Bi/MnBi₂Te₄ nanoribbon with P1 configuration. (d)-(f) same as (a)-(c) but for P1' configuration.

Strain effects

Beside the external magnetic field and twisting angle, applying an external strain is also an effective route to tune the material properties. We impose a biaxial strain ranging from -5% and 5% on both the P1 and P1' configurations of Bi/MnBi₂Te₄, and examine their relative energies, magnetic properties and topological features. As shown in Fig. 4, under a compressive strain, the magnetic easy axes of both P1 and P1' configurations are switched from in-plane to out-of-plane; meanwhile, the most stable alignment configuration changes from P1 to P1'. Note that, the topological properties as described in Fig. 3 are unchanged under a large range of strain, -4% ~ 5%, as long as we maintain the out-of-plane magnetization. Therefore, Bi/MnBi₂Te₄ not only displays IPM-QAHE with $C = \pm 1$, but also can be tuned to have robust OPM-QAHE with a high Chern number $C = \pm 3$. As these phases are switchable by means of biaxial strain or magnetic field, Bi/MnBi₂Te₄ is an ideal platform to realize tunable QAHE, similar to the NiAsO₃ and PdSbO₃ monolayers proposed recently by Li *et al.* [21].

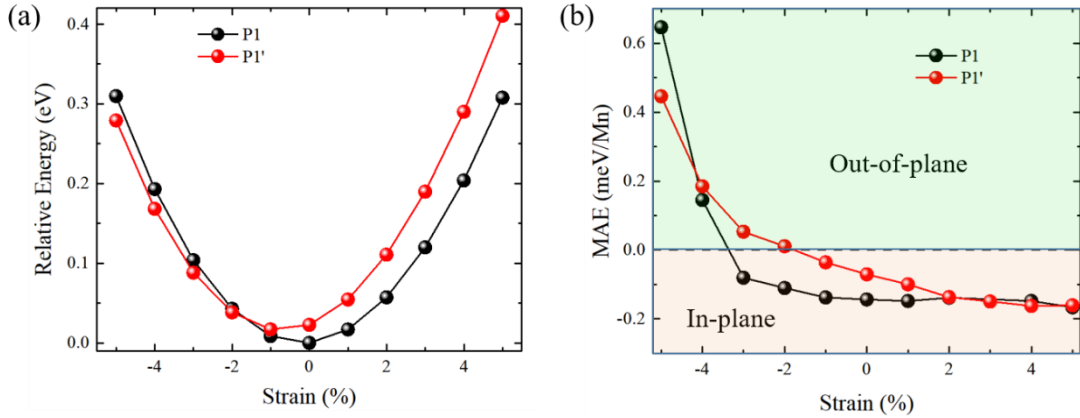


FIG 4. Strain effects on the relative energy and magnetic anisotropy energy (MAE) of P1 and P1' structures. (a) The relative energy and (b) MAE as a function of biaxial strain. The energy of P1 structure without strain is set to zero as a reference.

DISCUSSION AND CONCLUSION

Considering the vdW nature of MnBi₂Te₄ SL and Bi BL and their successful fabrications in experiments [35,36], we believe that the vdW Bi/MnBi₂Te₄ heterostructure is feasible for experimental synthesis [37]. On the other hand, ever since

the bulk MnBi_2Te_4 was theoretically identified as an intrinsic magnetic topological insulator [12,38,39], the OPM-QAHE has been extensively examined in MnBi_2Te_4 films, particularly for those thicker than 5 SLs [35,40]. A single MnBi_2Te_4 SL is a topologically trivial 2D FM semiconductor [12,39]. In this regard, it is of interest to realize QAHE in its heterostructure built with Bi BL and our finding of multiple QAHE phases in Bi/ MnBi_2Te_4 with such a thin thickness should be greatly beneficial for the design of ultra-thin topological spintronic devices [41].

In summary, based on systematic first-principles calculations, we demonstrate the highly tunable QAHE in a vdW heterostructure of 2D FM semiconductor MnBi_2Te_4 SL and nonmagnetic semiconductor Bi BL. We find that the Bi/ MnBi_2Te_4 heterostructure not only displays the unusual in-plane magnetization induced QAHE with a Chern number of $C = \pm 1$, but also has tunable QAHE with high Chern numbers of $C = \pm 3$ under out-of-plane magnetic fields. The interlayer twisting or biaxial strain may provide more means for the control of its topological phases. Specifically, the topological quantum phase transition from $C = \pm 1$ to $C = \pm 3$ and $C = +3$ to $C = -3$ can be realized in a single system by applying strain or perpendicular magnetic field. Our findings greatly extend the practical routes for searching materials with the highly tunable QAHE and should spur more experimental and theoretical explorations in this realm.

METHODS

As shown in Fig. 1(a), the Bi/ MnBi_2Te_4 heterostructure is modeled by a slab with a Bi BL on a single MnBi_2Te_4 SL layer. The lattice constant in the lateral plane was fixed to the optimized size of Bi BL, while the vertical positions of all atoms are relaxed. A vacuum space of 15 Å between adjacent slabs was set to eliminate the spurious interactions between periodic images. Density functional theory (DFT) calculations were performed by using the projector augmented wave [42,43] method as implemented in the Vienna *ab initio* simulation package (VASP) [44]. The exchange-correlation interaction was described by using the functional proposed by Perdew, Burke, and Ernzerhof (PBE) [45]. The semi-core states of Mn 3*p* and Bi 5*d* were treated as valence electrons. The cutoff energy of the plane-wave basis set was chosen to be 400 eV. A Γ -centered $15 \times 15 \times 1$ Monkhorst-Pack k-point mesh was adopted for structural relaxation, and a denser $23 \times 23 \times 1$ mesh was used for calculating their magnetic anisotropy energies. The structural relaxations were performed using the

conjugate gradient method with criteria that require the force acting on each atom smaller than 0.001 eV/Å and energy change less than 10^{-6} eV. The strong electron correlation effect for the localized orbitals of Mn was treated by the DFT+ U method [46] using $U = 4$ eV. The vdW corrections were invoked through the DFT-D3 method [47] in all calculations. In addition, the Heyd-Scuseria-Ernzerhof (HSE) hybrid functional was used [48] in test calculations. The edge state calculations were performed using the Wannier Tools [49], where the maximally localized Wannier functions were constructed by using the software package Wannier90 [50] interfaced with VASP.

FUNDING

This work was supported by the Ministry of Science and Technology of China (Grant Nos. 2018YFA0307100 and 2018YFA0305603), the Basic Science Center Project of NSFC (Grant No. 51788104), the National Science Fund for Distinguished Young Scholars (Grant No. 12025405), the National Natural Science Foundation of China (Grant Nos. NSFC-12104518 and 11874035), the Beijing Advanced Innovation Center for Future Chip, and the Beijing Advanced Innovation Center for Materials Genome Engineering. Work at the University of California, Irvine was supported by DOE-BES of USA (Grant No. DE-FG02-05ER46237). Computer simulations were partially performed at the U.S. Department of Energy Supercomputer Facility (NERSC).

References

1. Weng HM, Yu R, Hu X *et al.* Quantum anomalous Hall effect and related topological electronic states. *Adv Phys* 2015; 64: 227-82
2. Liu CX, Zhang SC, and Qi XL. The Quantum Anomalous Hall Effect: Theory and Experiment. *Annu Rev Condens Matter Phys* 2016; 7: 301-321
3. He K, Wang YY, and Xue QK. Topological Materials: Quantum Anomalous Hall System. *Annu Rev Condens Matter Phys* 2018; 9: 329-344
4. Yu R, Zhang W, Zhang HJ *et al.* Quantized Anomalous Hall Effect in Magnetic Topological Insulators. *Science* 2010; 329: 61-4
5. Zhang HB, Lazo C, Blügel S *et al.* Electrically Tunable Quantum Anomalous Hall Effect in Graphene Decorated by 5d Transition-Metal Adatoms. *Phys Rev Lett* 2012; 108: 056802
6. Chang CZ, Zhang JS, Feng X *et al.* Experimental observation of the quantum

- anomalous Hall effect in a magnetic topological insulator. *Science* 2013; 340: 167-70
7. Wang J, Lian B, Zhang HJ *et al.* Quantum Anomalous Hall Effect with Higher Plateaus. *Phys Rev Lett* 2013; 111: 136801
 8. Checkelsky J G, Yoshimi R, Tsukazaki A *et al.* Trajectory of the anomalous Hall effect towards the quantized state in a ferromagnetic topological insulator. *Nat Phys* 2014; 10: 731-6
 9. Kandala A, Richardella A, Kempinger S *et al.* Giant anisotropic magnetoresistance in a quantum anomalous Hall insulator. *Nat Commun* 2015; 6: 7434
 10. Feng Y, Feng X, Ou YB *et al.* Observation of the Zero Hall Plateau in a Quantum Anomalous Hall Insulator. *Phys Rev Lett* 2015; 115: 126801
 11. Hou YS, Kim J, and Wu RQ. Magnetizing topological surface states of Bi₂Se₃ with a CrI₃ monolayer. *Sci Adv* 2019; 5: eaaw1874
 12. Li J, Li Y, Du SQ *et al.* Intrinsic magnetic topological insulators in van der Waals layered MnBi₂Te₄-family materials. *Sci Adv* 2019; 5: eaaw5685
 13. Liu X, Hsu HC, and Liu CX. In-Plane Magnetization-Induced Quantum Anomalous Hall Effect. *Phys Rev Lett* 2013; 111: 086802
 14. Zhu T, Bishop A J, Zhou T *et al.* Synthesis, Magnetic Properties, and Electronic Structure of Magnetic Topological Insulator MnBi₂Se₄. *Nano Lett* 2021; 21: 5083-90
 15. Cai X, Song T, Wilson N P *et al.* Atomically Thin CrCl₃: An In-Plane Layered Antiferromagnetic Insulator. *Nano Lett* 2019; 19: 3993-8
 16. Vaz C, Bland J, and Lauhoff G. Magnetism in ultrathin film structures. *Rep Prog Phys* 2008; 71: 056501
 17. Bonilla M, Kolekar S, Ma Y *et al.* Strong room-temperature ferromagnetism in VSe₂ monolayers on van der Waals substrates. *Nat Nanotechnol* 2018; 13: 289-93
 18. Zhong P, Ren Y, Han Y *et al.* In-plane magnetization-induced quantum anomalous Hall effect in atomic crystals of group-V elements. *Phys Rev B* 2017; 96: 241103
 19. You J-Y, Chen C, Zhang Z *et al.* Two-dimensional Weyl half-semimetal and tunable quantum anomalous Hall effect. *Phys Rev B* 2019; 100: 064408
 20. Liu Z, Zhao G, Liu B *et al.* Intrinsic Quantum Anomalous Hall Effect with In-Plane Magnetization: Searching Rule and Material Prediction. *Phys Rev Lett* 2018; 121: 246401
 21. Li Z, Han Y, and Qiao Z. Chern Number Tunable Quantum Anomalous Hall Effect in Monolayer Transitional Metal Oxides via Manipulating Magnetization Orientation. *Phys Rev Lett* 2022; 129: 036801
 22. Yu Y, Chen X, Liu X *et al.* Ferromagnetism with in-plane magnetization, Dirac spin-gapless semiconducting properties, and tunable topological states in two-dimensional rare-earth metal dinitrides. *Phys Rev B* 2022; 105: 024407
 23. Wang J, Lian B, Zhang H *et al.* Quantum anomalous Hall effect with higher plateaus. *Phys. Rev. Lett.* 2013; 111: 136801
 24. Barkeshli M and Qi XL. Topological Nematic States and Non-Abelian Lattice Dislocations. *Phys Rev X* 2012; 2: 031013
 25. Gong C, Li L, Li Z *et al.* Discovery of intrinsic ferromagnetism in two-dimensional

- van der Waals crystals. *Nature* 2017; 546: 265-9
26. Huang B, Clark G, Navarro-Moratalla E *et al.* Layer-dependent ferromagnetism in a van der Waals crystal down to the monolayer limit. *Nature* 2017; 546: 270-3
 27. Burch K S, Mandrus D, and Park J-G. Magnetism in two-dimensional van der Waals materials. *Nature* 2018; 563: 47
 28. Gong C and Zhang X. Two-dimensional magnetic crystals and emergent heterostructure devices. *Science* 2019; 363: eaav4450
 29. Huang B, McGuire M A, May A F *et al.* Emergent phenomena and proximity effects in two-dimensional magnets and heterostructures. *Nat Mater* 2020; 19: 1276-89
 30. Xue F, Wang Z, Hou YS *et al.* Control of magnetic properties of MnBi₂Te₄ using a van der Waals ferroelectric III₂-VI₃ film and biaxial strain. *Phys Rev B* 2020; 101: 184426
 31. Aktürk E, Aktürk O Ü, and Ciraci S. Single and bilayer bismuthene: Stability at high temperature and mechanical and electronic properties. *Phys Rev B* 2016; 94: 014115
 32. Xiao S, Xiao X, Zhan F *et al.* Spin-polarized topological phases in a ferromagnetic Bi₂Te₃/MnBi₂Te₄ bilayer tuned by electric and magnetic fields. *Phys Rev B* 2022; 105: 125126
 33. Lee D S, Kim TH, Park CH *et al.* Crystal structure, properties and nanostructuring of a new layered chalcogenide semiconductor, Bi₂MnTe₄. *CrystEngComm* 2013; 15: 5532-8
 34. Bedoya-Pinto A, Ji JR, Pandeya A K *et al.* Intrinsic 2D-XY ferromagnetism in a van der Waals monolayer. *Science* 2021; 374: 616-20
 35. Deng Y, Yu Y, Shi MZ *et al.* Quantum anomalous Hall effect in intrinsic magnetic topological insulator MnBi₂Te₄. *Science* 2020; 367: 895-900
 36. Hirahara T, Bihlmayer G, Sakamoto Y *et al.* Interfacing 2D and 3D Topological Insulators: Bi(111) Bilayer on Bi₂Te₃. *Phys Rev Lett* 2011; 107: 166801
 37. Novoselov K S, Mishchenko A, Carvalho A *et al.* 2D materials and van der Waals heterostructures. *Science* 2016; 353: aac9439
 38. Zhang D, Shi M, Zhu T *et al.* Topological Axion States in the Magnetic Insulator MnBi₂Te₄ with the Quantized Magnetoelectric Effect. *Phys Rev Lett* 2019; 122: 206401
 39. Otkov MM, Rusinov IP, Blanco RM *et al.* Unique Thickness-Dependent Properties of the van der Waals Interlayer Antiferromagnet MnBi₂Te₄ Films. *Phys Rev Lett* 2019; 122: 107202
 40. Ge J, Liu Y, Li J *et al.* High-Chern-number and high-temperature quantum Hall effect without Landau levels. *Natl Sci Rev* 2020; 7: 1280-7
 41. Tokura Y, Yasuda K, and Tsukazaki A. Magnetic topological insulators. *Nat Rev Phys* 2019; 1: 126-43
 42. Blöchl P E. Projector augmented-wave method. *Phys Rev B* 1994; 50: 17953-79
 43. Kresse G and Joubert D. From ultrasoft pseudopotentials to the projector augmented-wave method. *Phys Rev B* 1999; 59: 1758-75
 44. Kresse G and Furthmüller J. Efficient iterative schemes for ab initio total-energy calculations using a plane-wave basis set. *Phys Rev B* 1996; 54: 11169-86

45. Perdew J P, Burke K, and Ernzerhof M. Generalized Gradient Approximation Made Simple. *Phys Rev Lett* 1996; 77: 3865-8
46. Dudarev S L, Botton G A, Savrasov S Y *et al.* Electron-energy-loss spectra and the structural stability of nickel oxide: An LSDA+U study. *Phys Rev B* 1998; 57: 1505
47. Grimme S, Antony J, Ehrlich S *et al.* A consistent and accurate ab initio parametrization of density functional dispersion correction (DFT-D) for the 94 elements H-Pu. *J Chem Phys* 2010; 132: 154104
48. Krukau A V, Vydrov O A, Izmaylov A F *et al.* Influence of the exchange screening parameter on the performance of screened hybrid functionals. *J Chem Phys* 2006; 125: 224106
49. Wu Q, Zhang S, Song HF *et al.* WannierTools: An open-source software package for novel topological materials. *Comput Phys Commun* 2018; 224: 405-16
50. Pizzi G, Vitale V, Arita R *et al.* Wannier90 as a community code: new features and applications. *J Phys Condens Matter* 2020; 32: 165902